Meas. Sci. Technol. **20** (2009) 115101 (12pp) doi:10.1088/0957-0233/20/11/115101

Wavelet-based estimator versus spectral correlation method for acoustic target sizing

A Scipioni[1], P Rischette[1,3], P Schweitzer[1] and J Mathieu[2]

[1] LIEN, Nancy Université, BP 239, F-54506 Vandoeuvre-lès-Nancy Cedex, France
[2] IUT de Rodez, 33 avenue du 8 mai 1945, F-12000 Rodez, France

E-mail: angel.scipioni@iut-longwy.uhp-nancy.fr, pascal.rischette@inet.air.defense.gouv.fr, patrick.schweitzer@lien.uhp-nancy.fr and mathieu@iut-rodez.fr

Received 21 April 2009, in final form 23 July 2009
Published 25 September 2009
Online at stacks.iop.org/MST/20/115101

Abstract
This paper presents two different methods for estimating the diameter of an immersed wire insonified by an ultrasonic plane wave. The first part of the backscattered echo, called the quasi-rigid backscattered echo (QRBE), and the quasi-rigid form function (QRFF) are described first. It is shown that the QRBE contains the size information (diameter) of the target. In the first method, this size is obtained by associating a pattern recognition procedure with a spectral correlation. The second method is based on a continuous wavelet analysis of the QRBE at a particular scale with a judiciously selected wavelet. After a brief description of the wavelet tool, we present in detail the wavelet-based approach for target sizing. Results thus obtained are compared with experimental measurements using copper and steel wires. They show that for the largest diameters, the results are similar. On the other hand, the more the diameter decreases, the more the wavelet-based estimator is distinguished by giving a better relative precision. In terms of the cost of calculation, the second method is better since it requires only one wavelet transform at only one single scale against a Fourier transform and an iterative correlation procedure, necessary in the first technique.

Keywords: wavelet, spectral correlation, target sizing, ultrasound

1. Introduction and motivation

The problems tackled in this paper are those of the sizing characterization by ultrasound of a target immersed in a liquid. This millimetric wire target is insonified by an ultrasonic broadband transducer, and our goal is to determine its diameter, by using two different methods which rely on the analysis of the backscattered echo. A possible application of these methods is the granulometry of particles in suspension in a liquid, in particular the measure of the volumetric rate of suspended solids in wastewater. Existing acoustic methods are based on the analysis of the attenuation spectrum [1]. However, the main disadvantage for all of these solutions is that the material of particles must be known. The granulometric methods proposed here are based on a backscattered echo study. Accordingly these could be used in continuous measures without solution sampling.

The study of the scattering of acoustic waves by a target has been made by several authors and more particularly the geometric and elastic waves analysis [2–8]. Resonance effects in acoustic echoes may be analyzed using the GTD [9] (geometrical theory of diffraction) or the RST [10] (resonant scattering theory). The latter, selected in the continuation of this work, shows that the backscattered echo is made up of several wave types which are particularly sensitive to the size and the physical nature of the target.

In preceding works [11], the authors established that the spectral composition of the first part (duration roughly equal to that of the incident impulse) of the backscattered echo produced by the target has the advantage of being strongly

[3] Present address: MorphoAnalysis in Signal processing Lab., Research Center of the French Air Force, BA701, F-13661 Salon air, France.

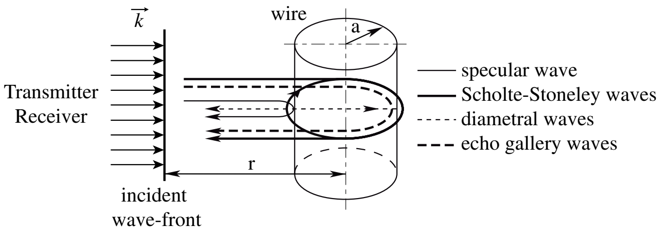

Figure 1. Nature of the waves crossing a target insonified by an ultrasonic wave.

dependent on the size of the target and of being only slightly affected by the nature of the material from which it is made.

The first method of radius estimation is based on the identification of the optimal parameter which ensures the best superimposition of the spectral backscattered echo segment on a function of reference. This method is similar to a technique of pattern recognition.

The second technique, also without contact, does not rely directly on the form function but on a family of synthetic echoes. Those are analyzed by a wavelet transform, more and more used in industrial applications [12], the coefficients of which are used as a foundation for the construction of a model, identifying the experimental signals.

The outline of this paper is as follows: section 2 points out some essential elements of the resonant scattering theory (RST) indispensable to a good understanding of the physical phenomena met. Section 3 presents the spectral method while section 4 details the time method. In section 5, we give a comparison of the differences in performance between these two estimating techniques.

2. Theoretical background

When a medium has acoustic impedance discontinuities limited in space, a phenomenon of scattering appears. This scattering results from the combination of various effects that are the reflection, the refraction and the diffraction of the ultrasonic waves on a target. An interpretation of these phenomena may be provided by the RST.

2.1. *Quasi-rigid backscattered echo*

The RST splits up the incidental wave into a sum of partial waves with respect to the geometry of the target and is strongly dependent on the wire's elastic and structural properties [13, 14]. Thus for a wire target, the incidental wave is broken up into various types of cylindrical waves as figure 1 shows.

Among the latter, the Franz waves (denoted as F_i^r: where r means rigid and i is the number of turns around the target) and Sholte–Stoneley waves [15, 16] (crawling waves) are dependent on the geometry and slightly affected by the nature of the target. Other waves (Rayleigh and whispering gallery waves, bulk waves), strongly dependent on acoustical properties of the immersed wire, compose the elastic part of the echo.

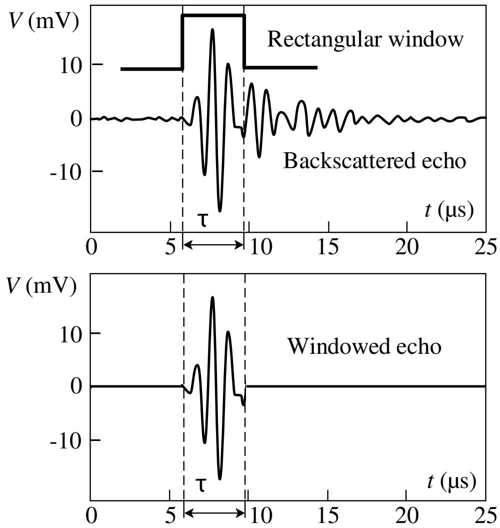

Figure 2. Complete and quasi-rigid echo.

Thus, in the ideal case of an infinitely rigid target, the first part of the echo backscattered by the target is made up only of the specular echo and the Franz waves.

In practice, we can observe only the Sholte–Stoneley waves, the Franz waves being too strongly attenuated [17].

On the one hand, for real targets, the more the reduced wave number ka increases (frequency bandwidth is imposed), the more the size of the target increases, and the more the crawling waves are delayed compared to the specular wave. On the other hand, when ka decreases, the quasi-rigid echo cannot be extracted properly from the whole echo because the elastic waves interfere.

The method explained below uses only the first part of the backscattered echo which contains mainly the radius information of the wire target. This part of the echo is called the quasi-rigid backscattered echo (QRBE) [11] and is obtained by a temporal windowing of duration equal to that of the incident pulse as shown in figure 2.

2.2. *Form function and acoustical transfer function*

With the aim of controlling the complexity of the equations which govern the phenomena of scattering, the material of the targets to be considered is solid, elastic, homogeneous and isotropic.

The incidental ultrasonic pressure wave to be considered is longitudinal, monochromatic, plane and with a wave vector $\vec{k}$.

The form function, so-called scattering magnitude, results from the theory of the collisions [18]. It is without unit and represents the variations of the magnitude of the wave scattered according to the observation angle θ and to the size a of the target compared to the wavelength ka (see figure 3). It also depends on the physical characteristics of the material and is related to the free modes of vibration [19]. It is denoted by $f(r, \theta, ka)$ when it is given at a distance r and as $f_\infty(\theta, ka)$ when $r \to \infty$.

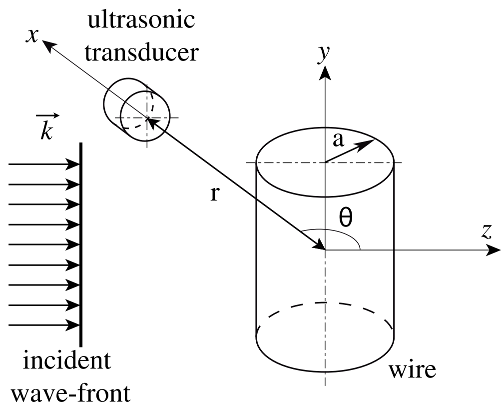

Figure 3. Ultrasonic insonification of a wire.

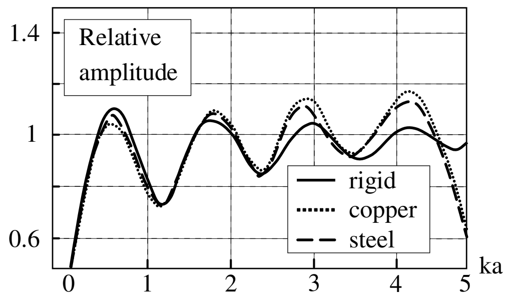

Figure 4. Quasi-rigid form function for wires.

In the case of a wire target and for $r \gg a$, the acoustic transfer function, which connects the incidental pressure and the backscattered pressure, is directly related to the form function and is expressed by [19]

$$H(r, \pi, ka) = \frac{P_s(r, \pi, ka)}{P_i(r, \pi, ka)} = \sqrt{\frac{a}{2r}} f_\infty(\pi, ka)\, e^{-2ikr}, \quad (1)$$

with

- $P_s(r, \pi, ka)$ and $P_i(r, \pi, ka)$ the Fourier transforms of the backscattered echo and the incident ultrasonic wave, respectively;
- $f_\infty(\pi, ka)$ the backscattered form function of the target;
- a the radius of the wire;
- k the wave number in the ambient medium;
- ka the reduced wave number and
- r the distance from the origin to the field point.

Contrary to the complete form function, there is no analytical expression of the quasi-rigid form function $f_{qr}(ka)$. The procedure for the calculation and construction of the quasi-rigid form function is widely explained in [20].

Figure 4 shows the results for a rigid wire and for wires made of copper and steel [20].

The good coincidence of the extrema of the quasi-rigid form functions for wire targets in the interval $ka \in [0.5, 3]$ confirms their slight dependence with respect to the physical nature of the material (figure 4). These functions are similar to the functions obtained for a rigid target. This last, denoted as $F(ka)$, is the reference function we use for estimating the radius of a target in the following parts using the spectral correlation method.

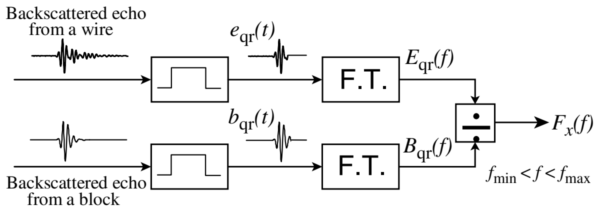

Figure 5. Schematic diagram to obtain the normalized quasi-rigid echo spectrum $F_x(f)$.

3. Diameter estimation using a spectral correlation method

3.1. Principle of the sizing method

The wire for which we estimate the diameter is insonified by a broadband transducer. Then we calculate the spectrum of the windowed backscattered echo by a short time Fourier transform to obtain $\mathrm{FT}[e_{qr}(t)]$. The same operation is done with the backscattered echo from a block sufficiently wide to simulate an infinite plane: $\mathrm{FT}[b_{qr}(t)]$. By dividing these two spectra in the limited bandwidth of the transducer ($f_{min} < f < f_{max}$), we obtain the normalized quasi-rigid echo spectrum $F_x(f)$. Thus, we eliminate the effects of transducer directivity (and other effects) as well as the attenuation of the medium [21]. This procedure is summarized by the diagram in figure 5.

We showed in [11] that by placing the segment $F_x(f)$ on the reference form function $F(ka)$ we obtain the estimate of the radius a (denoted as $\widehat{a}$) of the target. Our transducer having a finished and constant bandwidth (f_{min}, f_{max}), to each size corresponds an interval in the form function ($k_{min}a_j$ and $k_{max}a_j$). In the next section we present a correlation method to look for the optimal repositioning of the spectrum of the normalized backscattered quasi-rigid echo $F_x(f)$ on the reference form function $F(ka)$. This optimal repositioning allows us to estimate the radius of the wire target.

3.2. Spectral correlation method

Estimating the radius a of the wire consists of finding the optimal size for which the superimposition of the vector $F_x(f)$ on the form function of reference $F(ka)$ is the best.

The correlative method we present comprises several steps.

- From the reference form function $F(ka)$, we build a family of N functions $F_{a_j}(f)$ for each size, $a_j \in [a_0, a_{N-1}]$ with an incremental step equal to Δa.
- We denote by f_i $(0 \leqslant i \leqslant M-1)$ the discrete frequencies in the range $[f_{min}, f_{max}]$. This stage leads to the development of a matrix $\boldsymbol{X}$ (dim $M \times N$) formed of the values $F_{a_j}(f_i)$, and of a vector column $\boldsymbol{F}$ formed

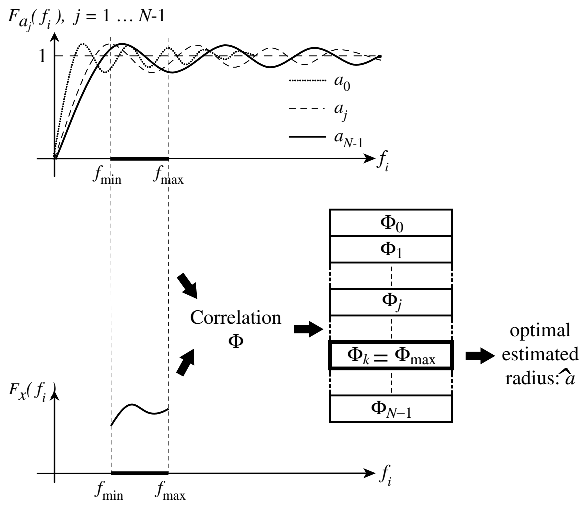

Figure 6. Diagram of the correlative method to obtain the best optimal size $\widehat{a}$ which ensures the best superimposition of the segment on the reference function.

of the values $F_x(f_i)$, as described below:

$$\boldsymbol{X} = \begin{pmatrix} F_0(f_0) & F_1(f_0) & \cdots & F_{a_{N-1}}(f_0) \\ F_0(f_1) & F_1(f_1) & \cdots & F_{a_{N-1}}(f_1) \\ \vdots & \vdots & & \vdots \\ F_0(f_i) & \cdots & \cdots & F_{a_{N-1}}(f_i) \\ \vdots & \vdots & & \vdots \\ F_0(f_{M-1}) & F_1(f_{M-1}) & \cdots & F_{a_{N-1}}(f_{M-1}) \end{pmatrix}, \quad (2)$$

$$\boldsymbol{F} = \begin{pmatrix} F_x(f_0) \\ F_x(f_1) \\ \vdots \\ F_x(f_{M-1}) \end{pmatrix}. \quad (3)$$

- We determine the vector $\boldsymbol{\Phi}$ of the correlations between the columns of $\boldsymbol{X}_{\mathrm{c}}$ and the vector $\boldsymbol{F}_{\mathrm{c}}$ using the relation
$$\boldsymbol{\Phi} = \boldsymbol{X}_{\mathrm{c}}^T \cdot \boldsymbol{F}_{\mathrm{c}}, \quad (4)$$
where $\boldsymbol{X}_c$ is the matrix $\boldsymbol{X}$ centered and reduced by column, and $\boldsymbol{F}_c$ is the vector $\boldsymbol{F}$ centered and reduced.
- Then we choose for the criterion of the best superimposition the maximum value of the components of vector $\boldsymbol{\Phi}$.

Figure 6 shows this procedure.

4. Diameter estimation using a wavelet-based estimator

4.1. Wavelet transform

The capability to provide the frequential composition of a stationary signal and the possibility of applying linear filtering operators to it make Fourier transform [22] an essential tool in signal processing. This decomposition of the signal is optimal in the sense that the imaginary exponentials of Fourier constitute a nonredundant analysis basis. However, the absence of localization of these functions allows only a global analysis of the signal and discredits this type of analysis in the sense of the uncertainty of Gabor–Heisenberg [23, 24]. Indeed, even if the short time Fourier transform (STFT) provides an undeniable improvement, the regularity of the time–frequency paving [25–27] which results from it is not relevant, as shown in figure 7. Moreover, the Fourier analysis being valid only for stationary signals is very badly adapted to the study of the transitory phenomena of a signal. The wavelet transform [28] provides multiple advantages.

- It enables one to approach the lower limit imposed by the uncertainty principle of Gabor–Heisenberg.
- The analysis basis of the wavelet transform uses functions perfectly located on the time–frequency plane.
- The great diversity of the functions offers an additional degree of freedom for the optimization of the number of coefficients produced by the analysis.
- In most cases, the richest information of a signal is located in its singularities (irregular structures). Wavelet transform allows exact analysis of local structures of the signal at the most relevant observation scale able to provide the available information.

The wavelet transform breaks up a signal f on a wavelet family translated (factor b) and dilated (factor a) starting from a mother wavelet ψ and forms an analysis basis being able to be orthonormal [29]. It is defined by

$$W[f_{a,b}] = \frac{1}{\sqrt{a}} \int_{-\infty}^{\infty} f(t)\psi^* \left(\frac{t-b}{a}\right) \mathrm{d}t \quad (5a)$$

$$\propto \langle f, \psi_{a,b} \rangle, \quad (5b)$$

where $\langle \cdot, \cdot \rangle$ means the inner product, $\propto$ denotes proportional to and ψ^* is the complex conjugate of ψ.

It must check the following essential properties.

- $\psi \in L^2(\mathbb{R})$,
$$\int_{\mathbb{R}} \psi(t)\, \mathrm{d}t = 0 \qquad \text{and} \qquad \int_{\mathbb{R}} \|\psi(t)\|^2\, \mathrm{d}t = 1. \quad (6)$$
- The functions generated by the mother wavelet ψ are
$$\psi_{a,b}(t) = \frac{1}{\sqrt{a}} \cdot \psi \left(\frac{t-b}{a}\right) \quad (7)$$
and allow an effective paving of the time–frequency plane. Thus, the operation measures the behavior of f around the moment b and in a radius proportional to the scale factor a.
- The mother wavelet ψ is characterized by a number of vanishing moments m such as
$$\langle t^m, \psi(t) \rangle = \int_{\mathbb{R}} t^m \psi(t)\, \mathrm{d}t = 0, \quad (8)$$
which is a decisive element in the description of the singularities of the signal f since the analysis will be blind with the polynomials of degree $m - 1$.

The continuous wavelet transform provides the most precise analysis on the time–frequency plane but at the price of a strong redundancy of appreciated information and thus of a strong cost of calculation [30]. There is an alternative allowing

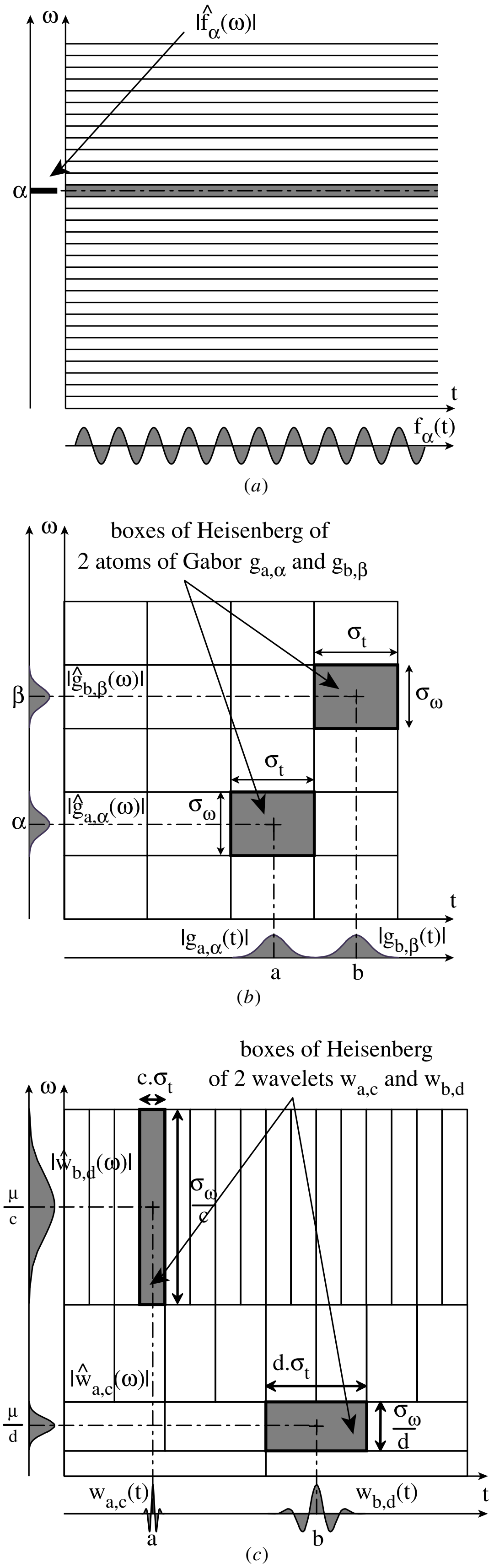

Figure 7. Time–frequency paving for boxes of Heisenberg of (*a*) Fourier transform, (*b*) short time Fourier transform (Gabor) and (*c*) wavelet transform.

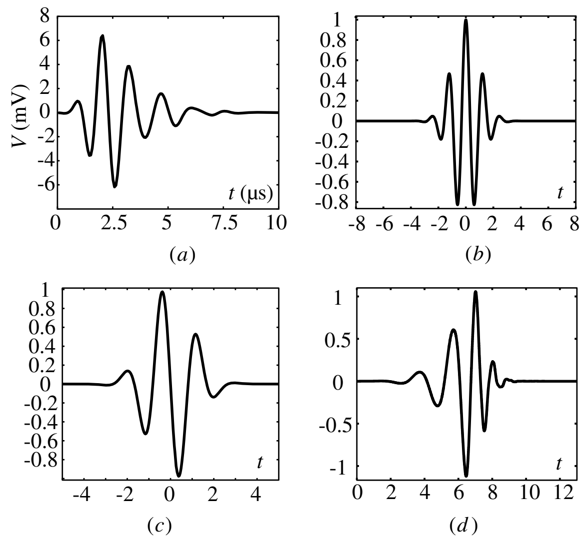

Figure 8. Morphological comparison: (*a*) synthetic quasi-rigid echo ($\emptyset = 0.5$ mm), (*b*) wavelet of Morlet, (*c*) wavelet of Gauss of order 7, (*d*) wavelet of Daubechies of order 7.

one to optimize the analysis by using wavelets generating discrete orthonormal bases of $L^2(\mathbb{R})$:

$$\left\{\psi_{j,n}(t) = 2^{\frac{-j}{2}}\psi(2^{-j}t - n)\right\}_{(j,n)\in\mathbb{Z}^2}. \tag{9}$$

That is how one constitutes a family of multiresolution approximations [31–33] of the signal f.

Multiresolution analysis (MRA) decomposes f by orthogonal projections on approximation V_j and detail W_j spaces [34] and this for all the possible resolutions 2^{-j}. The lost information between two scales 2^j and 2^{j+1} is entirely evaluated by the quantity $\sum_n \langle f, \psi_{j,n}\rangle \cdot \psi_{j,n}$.

Two discrete filters h and g facilitate the MRA's implementation and satisfy

$$h[n] = \langle \varphi, \varphi_{-1,n}\rangle_{n\in\mathbb{N}}, \tag{10}$$

where φ is the scaling function at scale $j = 0$,

$$g[n] = \langle \psi, \varphi_{-1,n}\rangle_{n\in\mathbb{N}}, \tag{11}$$

$$|\widehat{h}(\omega)|^2 = |\widehat{h}(\omega + \pi)|^2 = 2, \quad \text{with} \quad \widehat{h}(0) = 2. \tag{12}$$

These two filters constitute the quadrature mirror filters (QMF) and are at the base of Mallat's algorithm [35] which calculates the approximation and detail coefficients by

$$a_{j+1}[p] = \sum_{n\in\mathbb{Z}} h[n-2p]\cdot a_j[n] = a_j * \widetilde{h}[2p], \tag{13}$$

$$d_{j+1}[p] = \sum_{n\in\mathbb{Z}} g[n-2p]\cdot a_j[n] = a_j * \widetilde{g}[2p]. \tag{14}$$

4.2. *Principle of the sizing method*

The morphology of the experimental QRBE, whose experimentation conditions are described below, reminds one unequivocally of some wavelets as shown in figure 8. It thus appeared convenient to us to develop a characterization method of these signals, and more precisely a technique to estimate the wire target diameter, based on a wavelet analysis. However, in view of their great diversity, and as in most applications, the question of the wavelet choice is essential [36].

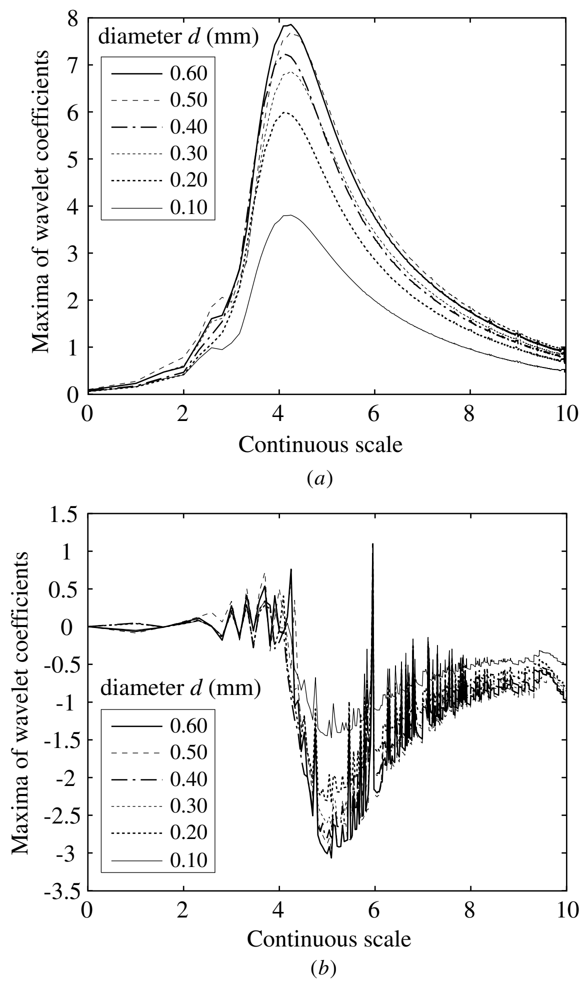

Figure 9. Maxima of the wavelet coefficients versus continuous scale for a wavelet of (*a*) Daubechies and (*b*) Morlet.

4.2.1. Wavelet selection. So as to choose the analyzing wavelet most appropriate to the characterization of the backscattered echoes, we undertook a systematic study whose objective was to find the wavelet which respects the following criterion.

- Maxima of wavelet coefficients, taken for each echo, and at a constant relevant scale, must respect a monotony relation between the diameters, as figure 9(*a*) shows for example on scale 4. Besides, we note in figure 9(*b*) that a wavelet does not necessarily respect this relation of order although it is morphologically adapted.

As seen in section 2, the QRBE is made up of the Sholte–Stoneley waves and the specular wave. The combination of these waves varies according to the diameter and thus also the width of the QRBE. That is the reason why it is necessary to find an constant interval, at the beginning of the backscattered echo, adapted to any diameter. The selected wavelet is the one which respects the criterion described above as often as possible for whatever part of the signal, be it its size or its position (cf figure 10(*a*)).

Figure 10(*b*) synthesizes the results and shows that two wavelets are distinguishable from others: 'sym2' and 'rbio2.2', a symlet of second order and a reverse β-spline 5/3 [28]. The first offers good behavior to the small parts of the signal but deteriorates as soon as the size increases (see figure 10(*a*)). On the other hand, the second is more robust and less sensitive to the signal size.

Moreover, it should be noted that the discrete wavelet transform did not allow finding a wavelet which respects in a robust way the monotony relation between the diameters and the wavelet maxima. That is the reason why the continuation of the method is based on a continuous wavelet transform with the 'rbio2.2' wavelet (CWT-rbio2.2). An interesting way would be to use the synthetic echoes as analysis wavelet. However, the behavior of this wavelet with regard to essential properties must be checked such as the time–frequency paving in the sense of Gabor–Heisenberg. Moreover, the impact of the loss of other important properties such as the number of vanishing moments must also be assessed.

4.2.2. Details of the method. As indicated in [11], it is possible to generate the theoretical backscattered echo of a wire corresponding to a given diameter, from its theoretical form function. We use this technique to create 11 synthetic backscattered echoes for diameters d (mm) $\in \{0.10, 0.15, 0.20, 0.25, \ldots, 0.6\}$, which are presented in figure 11 and which will be used as reference in the development of the estimator.

For the reasons described in the preceding paragraph, we must determine the part of the echo on which we will perform a CWT-rbio2.2. Thus, we must focus on the size and the position of this part of the echo.

On the size level, we must choose the part of the signal among all those which respect the monotony relation described above. For calculation costs and real time application reasons, we have chosen the shortest of these segments (10%).

With regard to the position of the lag in the signal, we have chosen the one which is located earliest in the echo (0.5%). Indeed, the QRBE being isolated from the complete echo after arbitrary windowing (see figure 2), possible remainders of elastic waves can more easily disturb the end than the beginning of this echo.

Then, we perform a CWT-rbio2.2 on this part of the echo, on each of the 11 synthetic echoes, by using the mirroring technique [37] aiming to reduce the edge effects, which leads to figure 12.

From these wavelet decompositions, one notes that all the maximum coefficients concentrate around scale 4, which allows one to have the representation of the diameter versus the maximum of wavelet illustrated in figure 13. Besides, it is necessary to emphasize here the surprising capacity of some wavelets to highlight the energy of each echo *for only one single scale*.

By minimizing the error in the sense of least-squares of a polynomial approximation, we obtain the expression of the model and thus the searched out estimator

$$d = 10^{0.014c_\mathrm{m}^3 - 0.048c_\mathrm{m}^2 + 0.181c_\mathrm{m} - 1.291}, \tag{15}$$

where d means diameter and c_m is the maximum of the wavelet coefficient.

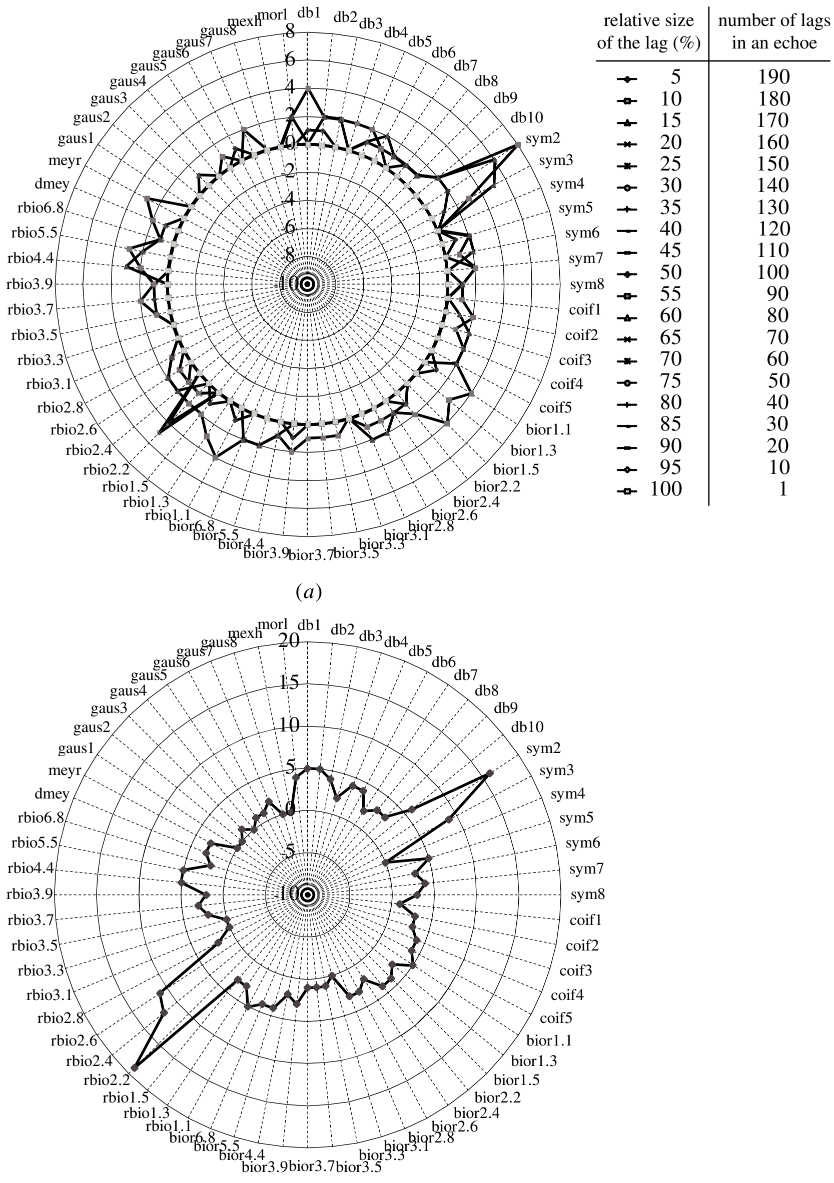

Figure 10. Number of respected monotony relations: (*a*) for several sizes and positions of the signal lag, (*b*) cumulated.

5. Comparison of the two methods

5.1. Experimentation

The measurements were carried out in a tank filled with water at ambient temperature. The experimental setup is shown in figure 14. The wires are fixed on a plexiglass framework in the axial beam of an ultrasonic transducer and a block of aluminum is used to calibrate the system.

The transmitter/receiver is a planar wideband transducer (−6 dB bandwidth: 0.8–1.4 MHz) with a diameter of 0.95 cm. Electrical excitation of the transmitter is provided by an Ultimo 2000 generator which delivers a negative impulse. The receiver gain can vary between −10 dB and 80 dB, and the impulse width can be adjusted between 25 ns and 1000 ns. The ultrasonic echoes are visualized on an oscilloscope Tektronix TDS 320. The bandwidth of the digital acquisition system is 100 MHz, and the sampling rate is 20 MS s^{-1}. The data are next acquired on a computer by an interface IEEE 488.2. The backscattered echoes for steel and copper wires of diameter d (mm) $\in \{0.25, 0.50, 1.00\}$ are presented in figures 15(*a*) and (*b*), respectively.

5.2. Diameter estimation by correlative analysis

5.2.1. Tests of good performance. The matrix $\boldsymbol{X}$ is built starting from the perfect rigid form function shown in figure 4 and the parameters summarized in table 1. To test our method, we chose for vector $\boldsymbol{F}$ one of the columns of $\boldsymbol{X}$. Thus we theoretically verify the possibility of estimating the radius a of the target.

The result presented corresponds to a test with a wire of radius 0.5 mm ($a_{90} = 0.5$ mm). Figure 16 describes the evolution of the vectors $\boldsymbol{F}$ and $\boldsymbol{\Phi}$. We have the maximum

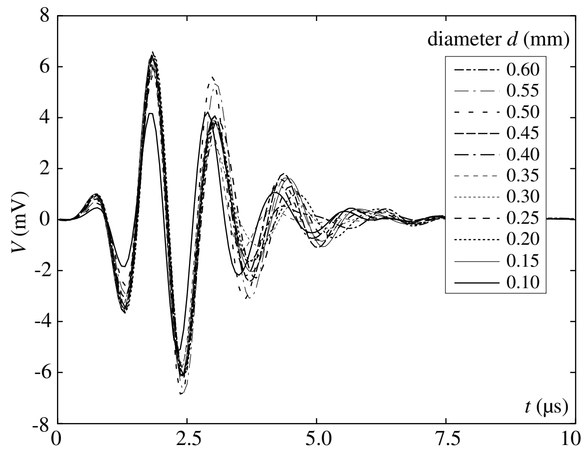

Figure 11. Synthetic echoes for a diameter d (mm) $\in$ {0.10, 0.15, 0.20, 0.25, . . . , 0.6}.

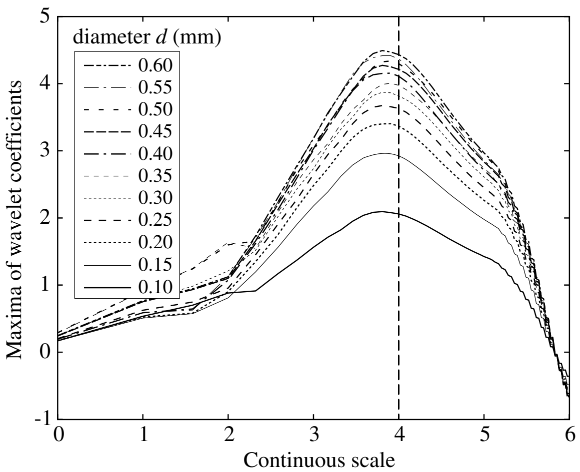

Figure 12. Maxima of the wavelet coefficients versus continuous scale for the wavelet rbio2.2.

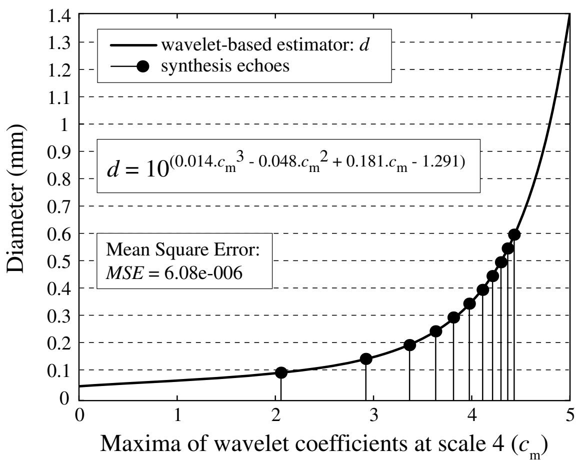

Figure 13. Construction of the wavelet-based estimator: distribution of the maxima of the wavelet coefficients for the synthetic echoes versus diameter, and the representation of the law existing between the diameter and the wavelet coefficients.

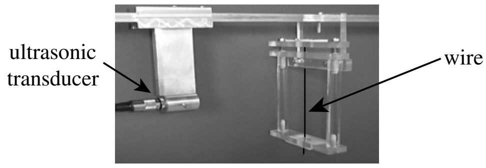

Figure 14. Experimental setup.

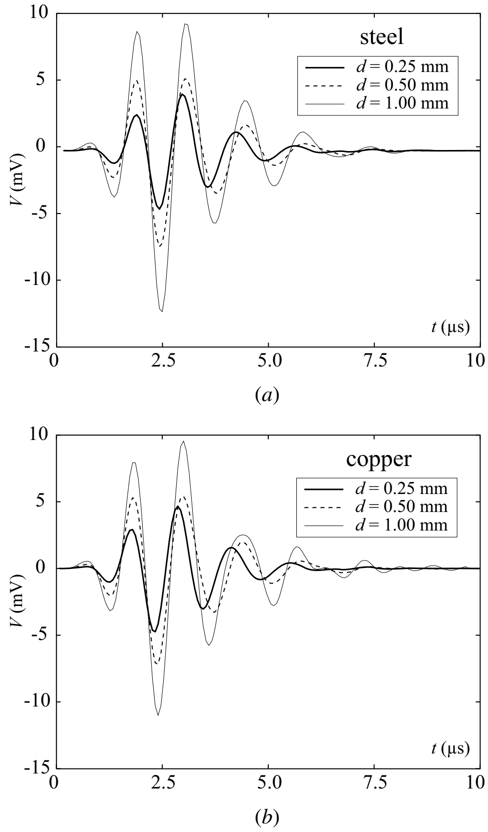

Figure 15. Experimental echoes for diameters (mm) $d \in \{0.25, 0.50, 1.00\}$ for wires of (*a*) steel and (*b*) copper.

Table 1. Parameters of the tests.

Frequency bandwith (kHz) $f_{\min} = 800$, $f_{\max} = 1400$ $\Delta f = 6$	Radii range a (mm) from 0.05 to 0.75 $\Delta a = 5 \times 10^{-3}$
Discrete frequencies f_i (kHz) $f_i = 800 + 6i$ $0 \leqslant i \leqslant 100$	Discrete radii a_j (mm) $a_j = 0.05 + 5 \times 10^{-3} j$ $0 \leqslant j \leqslant 40$

value of the vector components $\boldsymbol{\Phi}$ for $j = 90$ that corresponds to a good estimation of radius a. However, we have a risk of ambiguity related to the presence of secondary maximum for $\boldsymbol{\Phi}_j = 0.813$ where $j = 42$.

5.2.2. Influence of a limitation of the bandwidth. For a wire of radius 0.5 mm, we reduce the bandwidth of the transducer by 20% ($f_{\min} = 860$ kHz, $f_{\max} = 1340$ kHz). Figure 17 shows the limitation of the spectrum $\boldsymbol{F}$ and its effects on the function of correlation $\boldsymbol{\Phi}$. The maximum is always obtained for $j = 90$ but the amplitude of the secondary maximum increases $\boldsymbol{\Phi}_{42} = 0.946$. A bandwidth reduction increases the risk of a bad estimation, in particular when the measured radii are

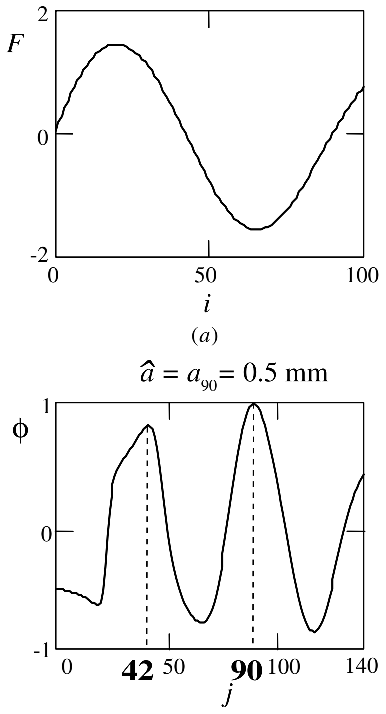

Figure 16. Shape of (*a*) vector $\boldsymbol{F}$ and (*b*) vector Φ.

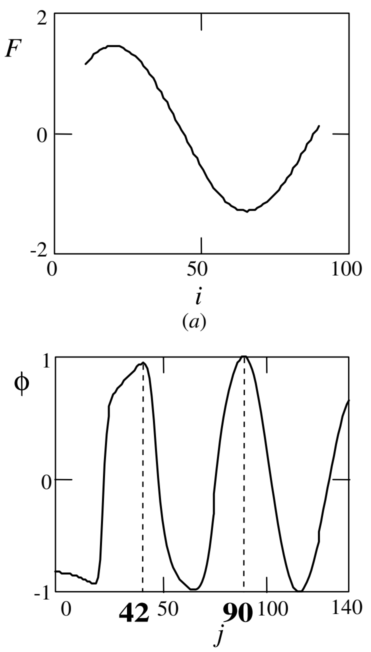

Figure 17. Shape of (*a*) vector $\boldsymbol{F}$, (*b*) vector Φ, when the bandwidth decreases.

weak. Thus, we find the theoretical limitations of resolution imposed by the spectral analysis.

5.2.3. Estimation results of the wire diameter. In these experiments, we applied our method to estimate three different wire diameters of steel and copper. Figure 18 represents the optimal superimposition of the vector $\boldsymbol{F}$ on the quasi-rigid

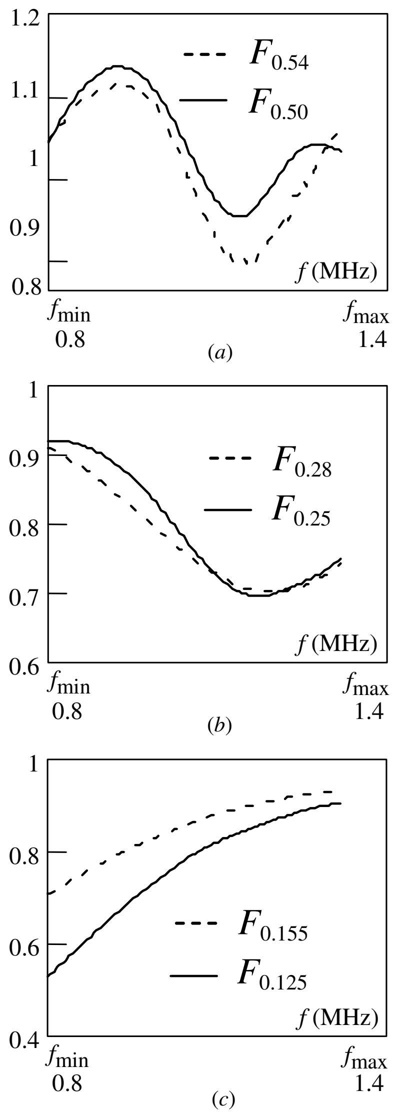

Figure 18. Superimposition of the segment on the form function of a steel wire: (*a*) $a = 0.500$ mm, (*b*) $a = 0.250$ mm, (*c*) $a = 0.125$ mm.

Table 2. Relative precision of the measurements.

Real radius (mm)	Material	Measured radius (mm)	Relative precision
∅ 0.500	Steel	0.54	8%
	Copper	0.56	12%
∅ 0.250	Steel	0.28	12%
	Copper	0.28	12%
∅ 0.125	Steel	0.15	24%
	Copper	0.16	28%

form function $F(ka)$ for steel wires of various diameters. The relative precision obtained for copper and steel wires is summarized in table 2.

The results obtained show that we have good precision for large radius. However, it deteriorates when the radius is below 0.25 mm. This situation was foreseeable because the segment $\boldsymbol{F}$ approaches a line and the method of correlation analysis

Table 3. Comparative results of the two methods for steel and copper wires of diameters 0.25, 0.50 and 1.00 mm.

Reference diameter (mm)	Computation methods	Steel			Copper		
		SCM[a]	WM[b]	Δ[c]	SCM	WM	Δ
∅ 0.25	Estimated value	0.31	0.23		0.32	0.24	
	Relative error	24%	8%	16%	28%	4%	24%
∅ 0.50	Estimated value	0.56	0.50		0.56	0.51	
	Relative error	12%	0%	12%	12%	2%	10%
∅ 1.00	Estimated value	1.08	1.02		1.12	0.92	
	Relative error	8%	2%	6%	12%	8%	4%

[a] Spectral correlation method.
[b] Wavelet method.
[c] Performance difference: SCM − WM.

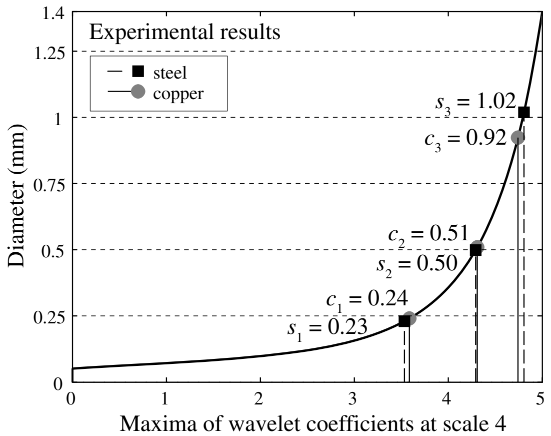

Figure 19. Validation of the wavelet-based estimator for steel and copper echoes.

is less adapted for the repositioning of this type of curve. A solution to address this defect would be either to increase the bandwidth of the transducer, or to complete the correlation with a least-squares analysis. In addition to the performance, the correlative method of analysis is totally independent of the scale factor of the measuring equipment.

5.3. Diameter estimation by wavelet analysis

The method is tested on the same experimental echoes as the correlative method and represented in figure 15. First of all, these backscattered echoes are normalized compared to the synthetic echoes of figure 11. For that, we use a point of measurement corresponding to $d = 0.4$ mm aiming at calculating the ratio of the magnitude differences and thus placing the echoes of the same diameter (theoretical and experimental) in the same magnitude range.

Then the mirroring technique is applied to the same lags of the signal as those selected for the synthetic echoes. Consequently, we can apply CWT-rbio2.2 and submit to the estimator the maximum of the coefficients at scale 4.

The results are presented in figure 19, in which we note that this method allows one to obtain good estimates of various diameters. Besides, it is interesting to emphasize that the model can also be applied to a value outside the range which is used for its development (between 0.1 and 0.6 mm). That is the case for the estimation of the 1 mm diameter.

5.4. Comparison and discussion

In regard to the principle, the two methods are rather clearly distinguished from each other: the first approaches the problem of dimensioning under the spectral angle while the second is placed under the time angle. However, more attentive observation shows that the second can be considered as an evolution of the first. Indeed, in terms of the choice of the analysis basis as in terms of localization, the wavelet transform of the second method is an improvement of the short time Fourier transform implemented in the correlative method. Moreover, in the two methods, the second phase of the processing is based on the development of a reference model. Thus in the first case, the QRBE to be analyzed is compared with the QRFF and in the second case, the wavelet maxima are subjected to a model built from the synthetic quasi-rigid echoes.

The two methods proposed provide good estimations in terms of precision and table 3 presents the results. Nevertheless, it is necessary to emphasize the better results of the wavelet method for all the diameters measured. Moreover, the relative variation of performance of the two methods increases when the diameters decrease.

The relative precision of the estimate for the correlative method varies between 8% and 28%. It tends to deteriorate when the diameter decreases. An improvement of the precision for the small diameters is possible by increasing the central frequency of the transducer, but at the price of a reduction of the possible diameter range ($ka < 3.5$).

In the case of the wavelet-based estimator, the relative precision is rather stable. It varies from 0% to 8% and does not seem to be sensitive to the reference diameter value.

6. Conclusion

Various applications, like granulometry for instance, require one to characterize particles immersed in a liquid. Here we propose two methods for estimating the target diameter belonging to the class of metals and based on the analysis of the backscattered ultrasonic echo. If the two methods use the quasi-rigid part of the experimental echo, they are characterized by two different approaches: one is articulated around a spectral correlation in connection with the QRFF, while the other exploits the time domain by a wavelet analysis associated with synthetic quasi-rigid echoes. Besides, we emphasize that this second approach is completely innovative since it is the first time that wavelets are used in this kind of application.

Experimental measurements showed that for the class of metals (i.e. with a high acoustic impedance) and for $ka < 3.5$, the QRBE spectrum is slightly sensitive to the nature of the material but strongly dependent on its diameter. This property allows the QRFF to become the reference to a spectral correlation. The estimate of the target diameter is obtained by finding the optimal superimposition between the QRFF and the QRBE spectrum of the wire to be measured. The second method is based on the morphological likeness between the QRBE and the used wavelets. It is remarkable to note that there exists, for a group of particular wavelets, a single scale containing the wavelet maxima relating to the diameters and respecting a monotony relation between them. It is this property, applied to synthetic quasi-rigid echoes, which allows the construction of a model of reference and which is the foundation of the wavelet-based estimator. In this case, the diameter estimate is obtained by subjecting to this model the wavelet maxima calculated on the QRBE of the wire to be measured.

If, in comparison with the other contactless methods of small target sizing, the two methods offer good-quality results, the wavelet-based method brings a decisive performance gain, particularly in terms of the calculation cost and especially in terms of result precision. We compared the two methods on steel and copper wires, with diameters ranging from 0.25 mm to 1 mm. With the correlative method, results deteriorate for small diameters. On the other hand, with the wavelet method the relative precision remains constant and always lower than 8% over the whole measuring range. Complementary studies are in hand and aim at extending the methods to other materials belonging to the same class and for a more significant number of targets covering a wider range of sizes. These methods of measurement can also be extended to spherical targets.

Acknowledgments

The authors would like to thank the referees for their helpful comments and suggestions.

References

[1] Alba F 1992 Method and apparatus for determining particle size distribution and concentration in a suspension using ultrasonics *US patent* No. 5121629
[2] Faran J J 1951 Sound scattering by solid cylinders and spheres *J. Acoust. Soc. Am.* **23** 405–18
[3] Flax L, Gaunard G and Überall H 1981 Theory of resonance scattering *Physical Acoustics: Principles and Methods* vol 15 ed W P Mason and R N Thurston (San Diego: Academic) pp 191–229
[4] Dickey J W, Frisk G V and Überall H 1976 Whispering gallery wave modes on elastic cylinders *J. Acoust. Soc. Am.* **59** 1339–46
[5] Dickey J W and Überall H 1979 Acoustic high-frequency scattering by elastic cylinders *J. Acoust. Soc. Am.* **66** 275–83
[6] Nümrich S K and Überall H 1992 Scattering of sound pulses and the ringing of target resonances *Physical Acoustics* vol 21 ed R N Thurston and A D Pierce (New York: Academic) pp 235–318
[7] Welton P J, de Billy M, Hayman A and Quentin G 1980 Backscattering of short ultrasonic pulses by solid elastic cylinders at large *ka* *J. Acoust. Soc. Am.* **67** 470–6
[8] Brill D and Gaunaurd G C 1983 Acoustic resonance scattering by a penetrable cylinder *J. Acoust. Soc. Am.* **73** 1448–55
[9] Marston P L 1988 Gtd for backscattering from elastic spheres and cylinders in water and the coupling of surface elastic waves with the acoustic field *J. Acoust. Soc. Am.* **83** 25–37
[10] Flax L, Dragonette L R and Überall H 1978 Theory of elastic resonance excitation by sound scattering *J. Acoust. Soc. Am.* **63** 723–31
[11] Mathieu J, Schweitzer P and Tisserand E 2002 Ultrasonic scattering technique for target size measurement *Meas. Sci. Technol.* **13** 660–6
[12] Truchetet F and Laligant O 2008 Review of industrial applications of wavelet and multiresolution-based signal and image processing *J. Electron. Imaging* **17** 031102
[13] Dragonette L R 1979 The influence of the Rayleigh surface wave on the backscattering by submerged aluminum cylinders *J. Acoust. Soc. Am.* **65** 1570–2
[14] Derem A, Rousselot J L, Maze J L, Ripoche J and Faure A 1982 Diffusion d'une onde acoustique plane par des solides immergés : étude expérimentale et théorique des résonances *Acustica* **50** 39–50
[15] Überall H 1973 Surface waves in acoustics *Physical Acoustics: Principles and Methods* vol 10 ed W P Mason and R N Thurston (New York: Academic) pp 1–60
[16] Rudgers A J 1969 Acoustic pulses scattered by a rigid sphere immersed in a fluid *J. Acoust. Soc. Am.* **45** 900–10
[17] Neubauer W 1973 Observation of acoustic radiation from plane and curved surfaces *Physical Acoustics: Principles and Methods* vol 10 ed W P Mason and R N Thurston (New York: Academic) pp 1049–61
[18] Bowman J J, Senior T B A and Uslenghi P L E 1987 *Electromagnetic And Acoustic Scattering Simple Shapes* (New York: Hemisphere)
[19] Dardy H D, Bucaro J A, Schuetz L S and Dragonette L R 1977 Dynamic wide bandwidth acoustic form-function determination *J. Acoust. Soc. Am.* **62** 1373–6
[20] Mathieu J, Schweitzer P, Tisserand E and Bellefleur D 2002 The backscattering and the quasi-rigid backscattering form functions: simulations and experimental validations *Acta Acust.* **88** 879–85
[21] Dragonette L R, Nümrich S K and Frank L J 1981 Calibration technique for acoustic scattering measurements *J. Acoust. Soc. Am.* **69** 1186–9
[22] Bracewell R N 1978 *The Fourier Transform and Its Applications* (New York: McGraw-Hill)
[23] Gabor D 1946 Theory of communication *J. IEE* **93** 429–57
[24] Battle G 1988 Heisenberg proof of the Balian–Low theorem *Lett. Math. Phys.* **15** 175–7
[25] Rioul O and Flandrin P 1992 Time-scale energy distributions—a general class extending wavelet transforms *IEEE Trans. Signal Process.* **40** 1746–57
[26] Rioul O and Vetterli M 1991 Wavelets and signal processing *IEEE Signal Process. Mag.* **8** 14–35

[27] Daubechies I 1990 The wavelet transform, time–frequency localization and signal analysis *IEEE Trans. Inform. Theory* **36** 961–1005
[28] Daubechies I 1992 *Ten Lectures on Wavelets* (Philadelphia: SIAM) pp 146–56
[29] Daubechies I 1988 Orthonormal bases of compactly supported wavelets *Commun. Pure Appl. Math.* **41** 909–96
[30] Jones D L and Baraniuk R G 1991 Efficient approximation of continuous wavelet transforms *Electron. Lett.* **27** 748–50
[31] Abry P and Aldroubi A 1995 Designing multiresolution analysis type wavelets and their fast algorithms *J. Fourier Anal. Appl.* **2** 135–59
[32] Jawerth B and Sweldens W 1994 An overview of wavelet based multiresolution analyses *SIAM Rev.* **36** 377–412
[33] Mallat S 1989 Multifrequency channel decompositions of images and wavelet models *IEEE Trans. Signal Process.* **37** 2091–110
[34] Aldroubi A and Unser M 1993 Families of multiresolution and wavelet spaces with optimal properties *Numer. Funct. Anal. Optim.* **14** 417–46
[35] Mallat S 1989 A theory for multiresolution signal decomposition: the wavelet representation *IEEE Trans. Pattern Anal. Mach. Intell.* **2** 674–93
[36] Kadambe S and Boudreaux-Bartels G F 1991 A comparison of a wavelet functions for pitch detection of speech signals *IEEE Int. Conf. Acoust. Speech and Signal Process.* pp 449–52
[37] Jensen A and la Cour-Harbo A 2001 *Ripples in Mathematics* (Berlin: Springer) pp 127–50